On the Solar Wind Proton Temperature Anisotropy at Mars' Orbital Location

Christy L. Lentz[1], Alexandros Chasapis[2], Ramiz A. Qudsi[3], Jasper S. Halekas[4], Bennett Maruca[3], Laila Andersson[5], and Daniel N. Baker[6]

[1]University of Colorado at Boulder
[2]University of Colorado
[3]University of Delaware
[4]University of Iowa
[5]Laboratory for Atmospheric and Space Physics (LASP)
[6]University of Colorado Boulder

November 23, 2022

Abstract

The Mars Atmosphere and Volatile EvolutionN (MAVEN) spacecraft can act as an intermittent upstream solar wind monitor at ˜ 1.5 AU. To inspect the evolution of solar wind turbulence in the Martian exosphere, we have gathered proton (i.e., ionized hydrogen) temperature measurements taken by the Solar Wind Ion Analyzer (SWIA) onboard the MAVEN spacecraft. Here we investigate instabilities driven by the proton temperature anisotropy at Mars. We look at the temperature anisotropy $T_{[?]p}/T_{||p}$ (i.e., the ratio of the perpendicular proton temperature component to the parallel proton temperature component) and the parallel plasma beta, $\beta_{||p}$, to determine the active plasma instability mode. Furthermore, we report on the properties of turbulence near Mars' orbital location during upstream solar wind intervals from January 2015 to December 2016 (˜ 1 Martian year). We find that the probability distributions of ($\beta_{||p}$, R_p)-values are limited at $R_p > 1$ and $R_p < 1$. We also find evidence of intermittency implying nonlinear, non-homogeneous energy transfer. Additionally, spectral index values near the Kolmogorov scaling value are observed for the inertial range (10^{-4} Hz to 0.1 Hz).

On the Solar Wind Proton Temperature Anisotropy at Mars' Orbital Location

C. L. Lentz[1], A. Chasapis[1], R. A. Qudsi[2], J. Halekas[3], B. A. Maruca[2], L. Andersson[1], D. N. Baker[1]

[1]Laboratory for Atmospheric and Space Physics, University of Colorado, Boulder, CO, USA
[2]Department of Physics and Astronomy, University of Delaware, Newark, DE, USA
[3]Department of Physics and Astronomy, University of Iowa, Iowa City, IA, USA

Key Points:

- Microinstabilities play a role in limiting proton temperature anisotropy (both $\frac{T_{\perp p}}{T_{||p}} > 1$ and $\frac{T_{\perp p}}{T_{||p}} < 1$) upstream of Mars
- Probability Density Functions of magnetic field fluctuations exhibit intermittent structures present in upstream plasma at Mars
- Power Spectral Densities of magnetic field fluctuations demonstrate an inertial range with Kolmogorov scaling value of -5/3

Corresponding author: C. L. Lentz, christy.lentz@lasp.colorado.edu

Abstract

The Mars Atmosphere and Volatile EvolutionN (MAVEN) spacecraft can act as an intermittent upstream solar wind monitor at ~ 1.5 AU. To inspect the evolution of solar wind turbulence in the Martian exosphere, we have gathered proton (i.e., ionized hydrogen) temperature measurements taken by the Solar Wind Ion Analyzer (SWIA) onboard the MAVEN spacecraft. Here we investigate instabilities driven by the proton temperature anisotropy at Mars. We look at the temperature anisotropy $T_{\perp p}/T_{||p}$ (i.e., the ratio of the perpendicular proton temperature component to the parallel proton temperature component) and the parallel plasma beta, $\beta_{||p}$, to determine the active plasma instability mode. Furthermore, we report on the properties of turbulence near Mars' orbital location during upstream solar wind intervals from January 2015 to December 2016 (~ 1 Martian year). We find that the probability distributions of $(\beta_{||p}, R_p)$-values are limited at $R_p > 1$ and $R_p < 1$. We also find evidence of intermittency implying non-linear, non-homogeneous energy transfer. Additionally, spectral index values near the Kolmogorov scaling value are observed for the inertial range (10^{-4} Hz to 0.1 Hz).

Plain Language Summary

Radially emanating from the Sun, solar wind consists of highly ionized and strongly magnetized plasma. During its expansion, the solar wind develops into a turbulent flow. With increasing distance from the Sun, based on the thermodynamic adiabatic expansion law, one would expect the temperature of protons in the solar wind to decrease at a certain rate. Instead we see that protons are hotter than expected; and therefore some heating mechanism must be at work. Due to the fact that turbulence functions as a reservoir of energy, instabilities associated with turbulent flows can then disperse free energy by wave excitation; subsequently heating the plasma. For idealized situations, the local free energy content of the solar wind can be characterized by the proton temperature anisotropy. While there have been multiple spacecraft to characterize turbulence and proton temperature anisotropies at 1 AU, there exist limited opportunities to obtain these same measurements beyond this orbital location. To study the basic properties of turbulence and proton temperature anisotropies at Mars' orbital location, we used the Mars Atmosphere and Volatile EvolutionN (MAVEN) spacecraft.

1 Introduction

1.1 Turbulence in the Solar Wind

Solar wind is a supersonic and super Alfvénic plasma flow originating from the Sun. It is a continuously expanding plasma that is highly ionized and threaded with large scale magnetic fields (Bruno & Carbone, 2016). The thermodynamic adiabatic expansion law applied to proton temperatures in the solar wind would suggest that temperature declines with heliocentric distance as $T(r) \sim r^{-\frac{4}{3}}$. However, this is not the case, and solar wind evolves in a highly non-trivial way as it expands from the Sun (e.g., Matteini et al., 2007). There exist numerous observations to imply that some heating mechanism must be at work within the solar wind to supply the energy required to slow down the decay (Pine et al., 2020).

One potential explanation for this heating is turbulence. As the highly ionized and magnetized solar wind develops into a turbulent flow at large scales, it can act as a reservoir of energy. As eddies in the turbulent plasma interact, they break up into smaller eddies, undergoing what is known as an energy cascade. In this energy cascade, there is a net transfer of energy from large scales, where turbulence first develops, to small scales, where dissipative mechanisms convert turbulent energy to heat (Verscharen et al., 2019; Bruno & Carbone, 2016; Howes, 2008; Klein & Howes, 2015).

The turbulent effects of the plasma can be described in a magnetohydrodynamic (MHD) framework (Matthaeus & Goldstein, 1982). This flow can also be described by hydrodynamic turbulence described by Kolmogorov at low frequency and long wavelengths (A. N. Kolmogorov, 1941; A. Kolmogorov, 1941). Plasma instabilities and associated wave particle interactions play a role in all observations at 1 AU. However, studies of solar wind turbulence outside of 1 AU are limited by instrument capabilities. The exception being the Ulysses spacecraft (1990-2009), whose magnetic field observations were used to study anisotropies of the solar wind turbulence at 1.4 AU from the Sun (Horbury et al., 2008).

To inspect the evolution of solar wind turbulence and proton temperature anisotropies in and upstream of the Martian atmosphere, we have gathered magnetic field data (MAG; Connerney et al., 2015) and proton temperature measurements taken by the Solar Wind Ion Analyzer (SWIA; Halekas et al., 2015) both onboard the MAVEN spacecraft. Here we examine Probability Distribution Functions (PDFs) and Power Spectral Densities (PSDs) of magnetic field fluctuations to report on solar wind turbulence near Mars' orbital location. Furthermore, we investigate instabilities driven by the proton temperature anisotropy at Mars to determine the plasma instability modes most active. These results provide novel insights into the physics of solar wind around Mars and contribute to the understanding of the role turbulence and plasma instabilities play in the evolution of the solar wind.

1.2 The Martian Plasma Environment

Mars acts as an obstacle to the supersonic and magnetized plasma emanating from the Sun. A shock wave is formed in front of the planet known as the bow shock. It serves to slow down the flowing solar wind from supersonic to subsonic speeds (Luhmann, 1992; Mazelle et al., 2004). Plasma thermalization then occurs in the sheath, at and downstream of the shock (Luhmann, 1992).

One fascinating feature of Mars is an exosphere that extends beyond the bow shock due to the weaker gravity of the planet (Mazelle et al., 2004). Above the exobase (altitude $\sim$ 200 km; Bhattacharyya et al., 2017) an extended exosphere is formed in part due to the ballistic motion of hydrogen atoms (Anderson, 1974; Anderson and Hord, 1971; Chaufray et al., 2008; Feldman et al., 2011; Chaffin et al., 2015). There is known to be a high degree of variability of the hydrogen density of the exosphere, with peak hydrogen densities occurring at Solar Longitude (L_s) values $\sim$ 263-288°, roughly centered on Mars southern summer solstice ($L_s = 270°$; Halekas, 2017). Where L_s is the Mars-Sun angle measured from the Northern Hemisphere spring equinox ($L_s = 0°$). This causes the solar wind/Mars interaction and therefore upstream dynamics at Mars to be very complex.

Further differences between plasma properties at Earth and Mars arise from Mars' greater heliocentric distance and its smaller size. The lower solar wind density and interplanetary magnetic field (IMF) strength makes for a different Mach number. Due to the smaller planet size and diminished IMF strength, the gyroradius of solar wind protons is comparable to the size of the shock, making kinetic effects important (Mazelle et al., 2004).

Few studies have investigated turbulence at Mars. Ruhunusiri et al. (2017) was the first known study to characterize turbulence in the Mars plasma environment. They determined that turbulence characteristics at Mars vary seasonally. Additionally, they found that a fully developed energy cascade is absent in the magnetosheath of Mars, but present in the magnetic pileup boundary (also known as the induced magnetosphere boundary; see Espley (2018) for a debate on the nomenclature). A study conducted by Andrés et al. (2020) estimated the incompressible energy cascade rate at MHD scales in the plasma upstream of the bow shock for events with and without proton cyclotron wave (PCW) activity. To date, there have been no known studies looking into the proton temperature anisotropy at Mars, and therefore this article aims to provide an evaluation of temperature anisotropy instabilities.

2 Methodology

2.1 Data

In order to analyze plasma instabilities and associated wave-particle interactions at Mars' orbital location, we used SWIA to obtain 3D distributions of proton temperature moments. SWIA is an electrostatic analyzer designed to measure solar wind and magnetospheric ions in the Martian planetary environment. Among other quantities, temperature is calculated on board from SWIA coarse data when MAVEN is in the sheath, or fine data when MAVEN is in its solar wind mode. A few caveats of note are that moments are computed assuming the entire distribution is within the field of view and energy range of SWIA. Also, the assumption that all ions are protons is made which can be problematic when looking into the data quantitatively. The upstream solar wind consists of $\sim$ 94-97% protons and $\sim$ 3-6% alpha particles. Any alpha particles present in the distribution, which SWIA is using to compute the temperature moment, can lead to artificially large values. This effect is most prominent in the component of the temperature moment that is aligned with the flow. Another potential hiccup arises when attempting to completely resolve temperatures when cold plasma beams are being sampled. This is due to the $\sim$ 15% energy resolution of SWIA. Not all hope is lost however, as proton temperatures can be calculated by taking SWIA level 2 3D fine data and separately computing proton and alpha temperature moments using a routine discussed in (Halekas et al., 2017).

Alpha particles are typically separated along the magnetic field from the protons. By locating proton and alpha peaks in the 3D distributions, the energy in between them can be bisected. Everything on the alpha side of the break is then disregarded, and the proton moments are then calculated. When thermal velocity is small compared to bulk velocity, alpha particles show up at twice the energy per charge than protons, and therefore can be separated. This is challenging to do so with really hot distributions, as SWIA does not have mass resolution capabilities. This causes difficulty in discerning proton and alpha peaks because they overlap in hot distributions. Besides these caveats, the routine successfully generates x, y, and z components of proton temperatures in magnetic field aligned coordinates. The z component is then $T_{||p}$, or the parallel proton temperature component. The average of x and y components is taken to be $T_{\perp p}$, or the perpendicular temperature component.

MAG measurements were used to calculate the parallel plasma beta component, $\beta_{||p}$, and to facilitate solar wind interval identification. Two tri-axial fluxgate magnetometer sensors measure the vector magnetic field throughout the Martian plasma environment over a wide dynamic range with a resolution up to 0.008 nT at an accuracy of around 0.05%. The better of the two magnetometers are used to sample the ambient magnetic field at a rate of 32 vector samples per second and create the standard data product.

Although it is debatable if MAVEN's orbit ever encounters truly pristine upstream solar wind at Mars due to the exosphere, there is still plenty of information that can be gleaned about turbulence and temperature anisotropies. An example of a manually identified upstream solar wind period on January 9th 2015 using SWIA and MAG measurements is shown in Figure 1. Panel a) displays the x, y, and z position coordinates of MAVEN, along with the altitude in units of Mars radii using the Mars-Sun-Orbital (MSO) coordinate system (see Slavin and Holzer (1981) page 11,404 for a detailed explanation on MSO coordinate system). Panel b) shows the magnetic field vector measurements in MSO coordinates ($\vec{B}_x$, $\vec{B}_y$, and $\vec{B}_z$), the magnitude of the magnetic field ($|\vec{B}_{sw}|$), and the inverse of the magnitude of the magnetic field($-|\vec{B}_{sw}|$). Panel c) shows SWIA measured

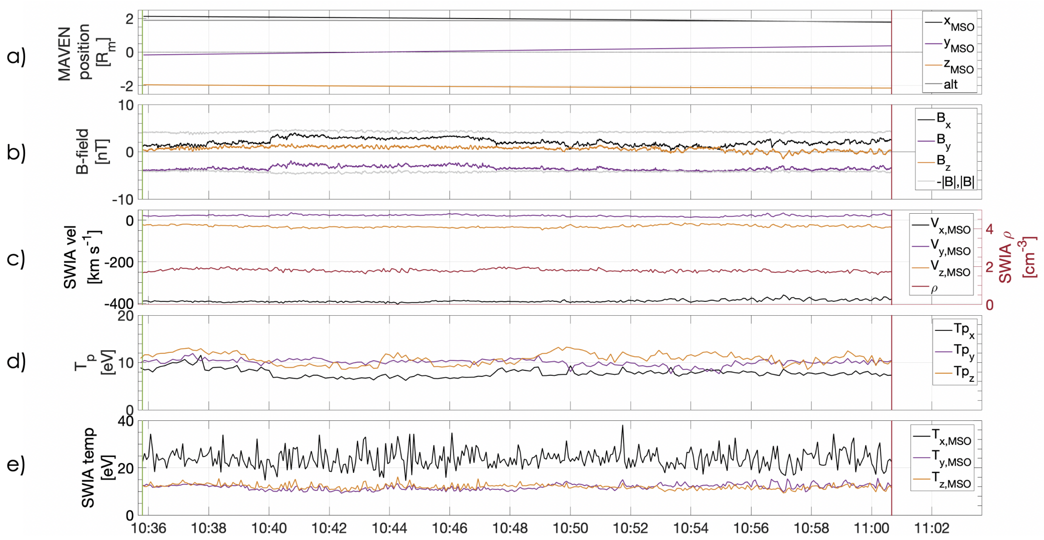

Figure 1. A solar wind interval manually identified from January 9, 2015. Panel a) shows MAVEN position in MSO coordinates in units of Mars radii obtained from key parameters data set. Panel b) shows the magnitude of the magnetic field, $|B|$, inverse $|B|$, the Bx, By, and Bz components in MSO coordinates. Panel c) shows SWIA velocity component measurements in MSO coordinates (left axis), and SWIA density measurements (right axis). Panel d) shows calculated proton temperature measurements. Panel e) onboard SWIA temperature moments.

MSO velocity coordinates on the left axis, and ion density measurements on the right axis. Panel d) shows the computed proton temperature measurements. Panel e) shows the SWIA temperature moments calculated onboard.

Upstream solar wind intervals were identified for the 1st through the 10th of each month from January 2015 to December 2016. The number of intervals each month were limited by the availability of the proton temperature moments. Upstream solar wind periods at Mars were recognized in the magnetic field by diminished fluctuations in the magnetic field components, and low vector magnitude ($|\vec{B}_{sw}| \leq 10$ nT) compared to other plasma regions and boundaries. Also, the typical density rose no higher than 10 protons per cubic centimeter ($\rho \leq 10$ cm^{-3}). There was also a steady negative x component of the velocity ($\vec{V}_x < 0$).

From these intervals turbulent statistics and temperature anisotropies were then calculated. To access the start and stop times along with maxima, minima, medians, and averages of every parameter discussed in this study, please reference the supplementary material. The solar wind intervals were then classified into southern hemisphere Martian seasons using the L_s values. $0 < L_s < 89°$ represents the Martian fall season, $90 < L_s < 179°$ corresponds to winter, $180 < L_s < 269°$ corresponds to spring, and $270 < L_s < 359°$ corresponds to summer. For this study, 2015-07-01 to 2016-01-03/02:22:08 corresponded to autumn. Winter months were 2016-01-03/02:22:16 - 2016-07-04/15:39:44. Spring mapped to the time periods 2015-01 and from 2016-07-04/15:39:52 to 2016-11. Summer months were from 2015-02 to 2015-06, and 2016-12.

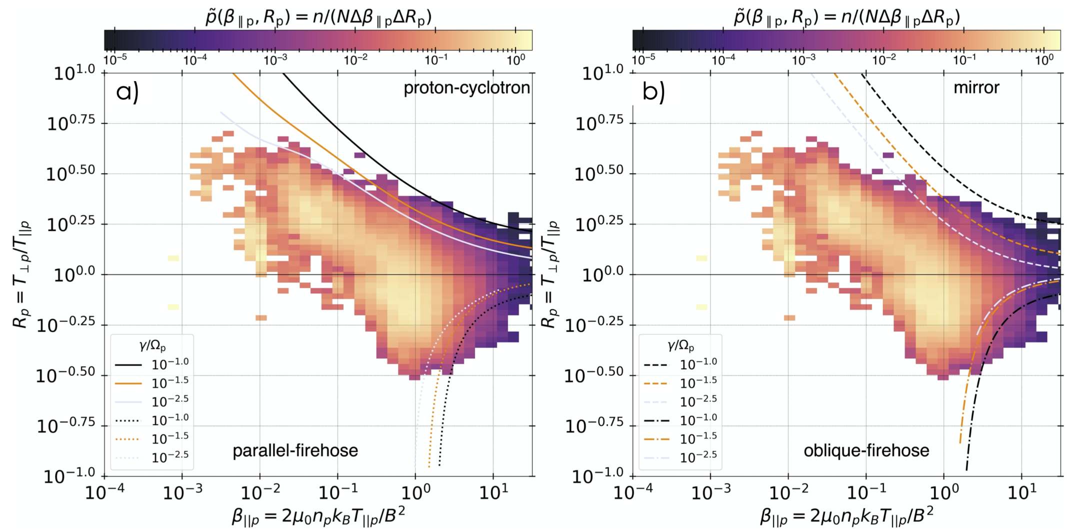

Figure 2. Probability distributions of $(\beta_{||p}, R_p)$-values from January 2015 to December 2016. a) depicts probability distributions with contours of constant growth rate (in units of proton cyclotron frequency $[\Omega_p]$) for parallel instabilities. The solid lines in the upper right corner of a) represent constant growth rates for the proton-cyclotron instability, while the dotted lines represent the parallel-firehose instability. The dashed lines in b) show the mirror instability, while the dot-dashed lines show the oblique-firehose instability.

3 Results

3.1 Probability distributions of $(\beta_{||p}, R_p)$-values

Due to the solar wind's strong magnetic field, the transport of energy is direction dependent, which can bring about temperature anisotropy. The temperature anisotropy in protons can be described by the following ratio.

$$R_p = \frac{T_{\perp p}}{T_{||p}} \tag{1}$$

Where R_p is the ratio of the proton temperature component perpendicular to the local mean magnetic field ($T_{\perp p}$), to the proton temperature component parallel to the magnetic field ($T_{||p}$). The distribution of R_p values observed in the solar wind depend strongly on the ratio of the parallel proton pressure to the magnetic pressure, known as the parallel plasma beta (Maruca et al., 2018).

$$\beta_{||p} = \frac{n_p k_B T_{||p}}{|\vec{B}_{sw}|^2/(2\mu_0)} \tag{2}$$

Where n_p is the proton density, k_B is the Boltzmann constant, and μ_0 is the vacuum permeability.

A R_p value of 1 corresponds to temperature isotropy (i.e., a state of equilibrium). If R_p deviates from unity, proton temperature anisotropy may prompt various plasma instabilities. Some commonly known instabilities such as the proton-cyclotron instability and/or the mirror instability arise when the perpendicular proton temperature component is larger than the parallel proton temperature component ($T_{\perp p} > T_{||p}$). However, when the parallel proton temperature component is larger than the perpendicu-

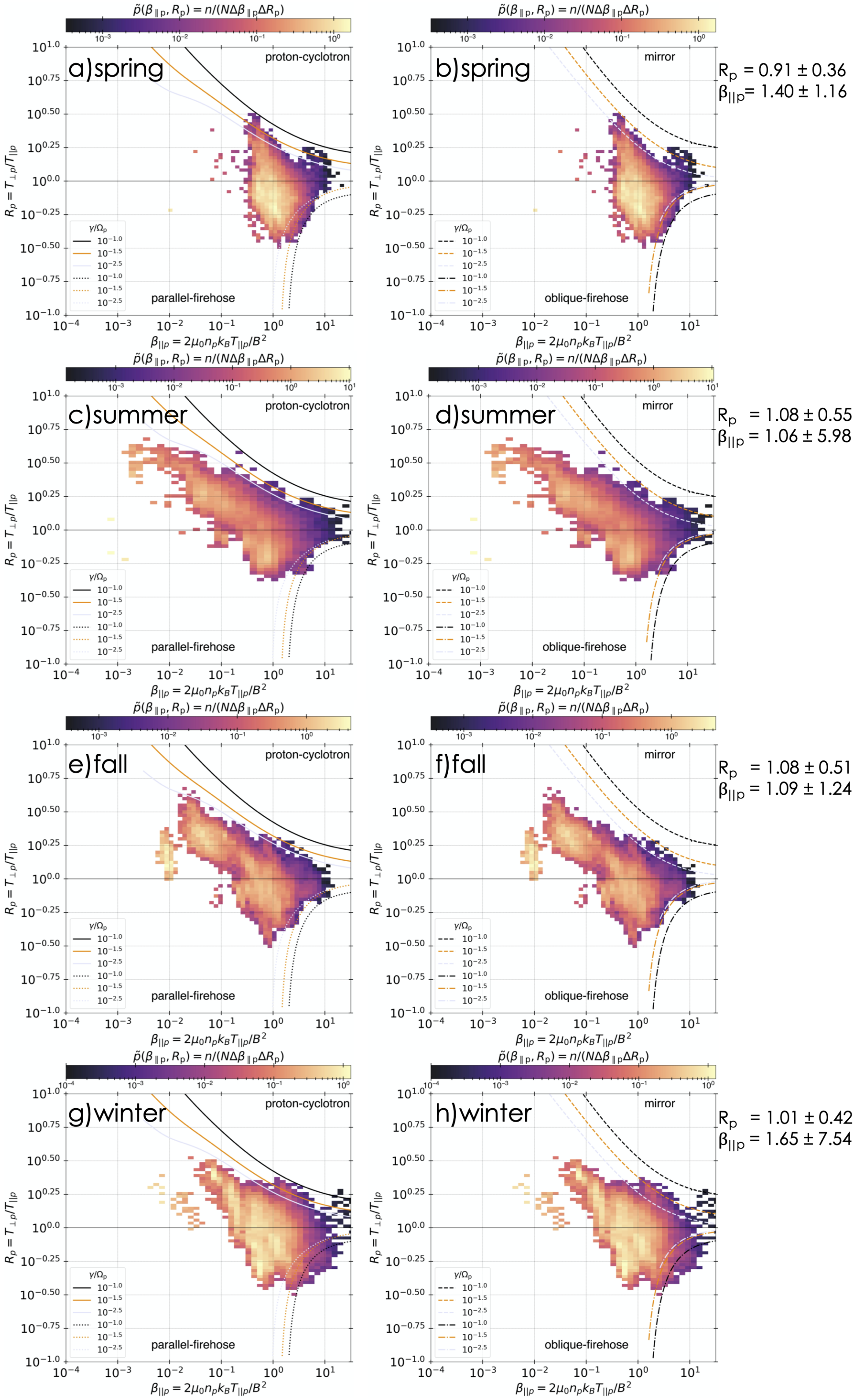

Figure 3. Probability distributions of $(\beta_{||p}, R_p)$-values for each Martian southern hemisphere season examined. a), c), e), and g) display probability distributions for parallel instabilities for spring, summer, fall and winter. b), d), f), and h) display probability distributions for perpendicular instabilities for spring, summer, fall and winter. Included to the right of all plots are the average plus/minus the standard deviation of R_p and $\beta_{||p}$.

lar proton temperature component ($T_{||p} > T_{\perp p}$), the parallel and/or the oblique firehose instabilities may arise.

To search for the effects of various instabilities, the approach outlined in Maruca et al. (2018) was used to plot the distribution of observations over the $(\beta_{||p}, R_p)$-plane using equations 1 and 2. The $(\beta_{||p}, R_p)$-plane is a tool to study the impact of anisotropy-driven instabilities on protons in the solar wind.

Figure 2 displays the probability distributions of $(\beta_{||p}, R_p)$-values $[\tilde{p}(\beta_{||p}, R_p)]$ for the entire study. Figure 3 displays $\tilde{p}(\beta_{||p}, R_p)$ for each season. The average $\pm$ the standard deviation of R_p and $\beta_{||p}$ are also displayed to the right of each season. The overlaid curves in both figures show the contours of constant growth rate (γ) for different instabilities, normalized by the proton frequency (Ω_p). Following the method originally outlined in Maruca et al. (2011), the growth rate of an instability is taken to be the growth rate of its fastest-growing wave mode. An instability is defined as being active if some wave modes are growing ($\gamma > 0$). Growth rates of anisotropy-driven instabilities are dependent upon $\beta_{||p}$ and R_p values. Therefore a common analysis technique is to plot contours of constant γ in the $(\beta_{||p}, R_p)$-plane. $\gamma(\beta_{||p}, R_p)$ is taken to be the growth rate of the fastest-growing mode for that set of values and is normalized to the proton frequency, $\Omega_p = q_p B/m_p$, where q_p is the charge and m_p is the mass of a proton. All of these contours were calculated using the linear Vlasov software described by Maruca et al. (2012), which considers an idealized plasma where each population of particles has a biMaxwellian velocity distribution function. For the present study, electrons were assumed to be isotropic. Likewise, the presence of proton beams and α-particles was neglected.

3.2 Turbulence at Mars

The study of temperature anisotropy in conjunction with turbulence at Mars' orbital location was motivated by such studies as Osman et al. (2012, 2014). The authors provided evidence that a turbulent cascade from inertial to kinetic scales is the causal agent allowing the solar wind to populate the extremes of the $(\beta_{||p}, R_p)$-plane. They suggested that while instabilities may act to confine the solar wind plasma, turbulent fluctuations and cascade rates can cause temperature anisotropies, intermittent structures, and heating in the $(\beta_{||p}, R_p)$-plane.

Intermittent structures are a feature of turbulence. One way to quantify intermittency of turbulence is to calculate the probability distribution function (PDF). PDFs of turbulent quantities are Gaussian, but the PDFs of increments of a turbulent quantity are not. By taking the increments of the magnetic field components ($\delta B_i(t,\tau) = B_i(t) - B_i(t+\tau)$), we can highlight the gradients or high magnetic stress and coherent structures (Osman et al., 2012), and hence the intermittent structures present (Parashar et al., 2015; Sorriso-Valvo et al., 1999). Observations of intermittency imply that a nonlinear, non-homogeneous energy transfer is going on. Here the subscript i represents the x, y, or z magnetic field component, and τ represents the lag. Figure 4 displays the normalized PDFs of magnetic field fluctuations for each Martian season. Each PDF of increments is normalized using $(\delta B_i(t,\tau) - \langle \delta B_i(t,\tau) \rangle)/\sigma_i$ where σ_i represents the standard deviation of $\delta B_i(t,\tau)$. Intermittency is highlighted by heavy tails in the PDFs of increments, and is present in all four seasons.

The solar wind is a highly variable environment, and extreme values of increments can be present, such as the tails shown throughout Figure 4. The inertial range solar wind PDF is known to have a typical shape with a narrow peak and fat tails (Marsch & Tu, 1997). The strength of the gradients highlighted depends on the lag τ. Smaller values of τ help highlight gradients (i.e., intermittent structures). When τ becomes comparable to the correlation length of the system, the PDFs revert back to Gaussianity. It has been shown that the non-Gaussian tails on the PDFs of increments correspond to the

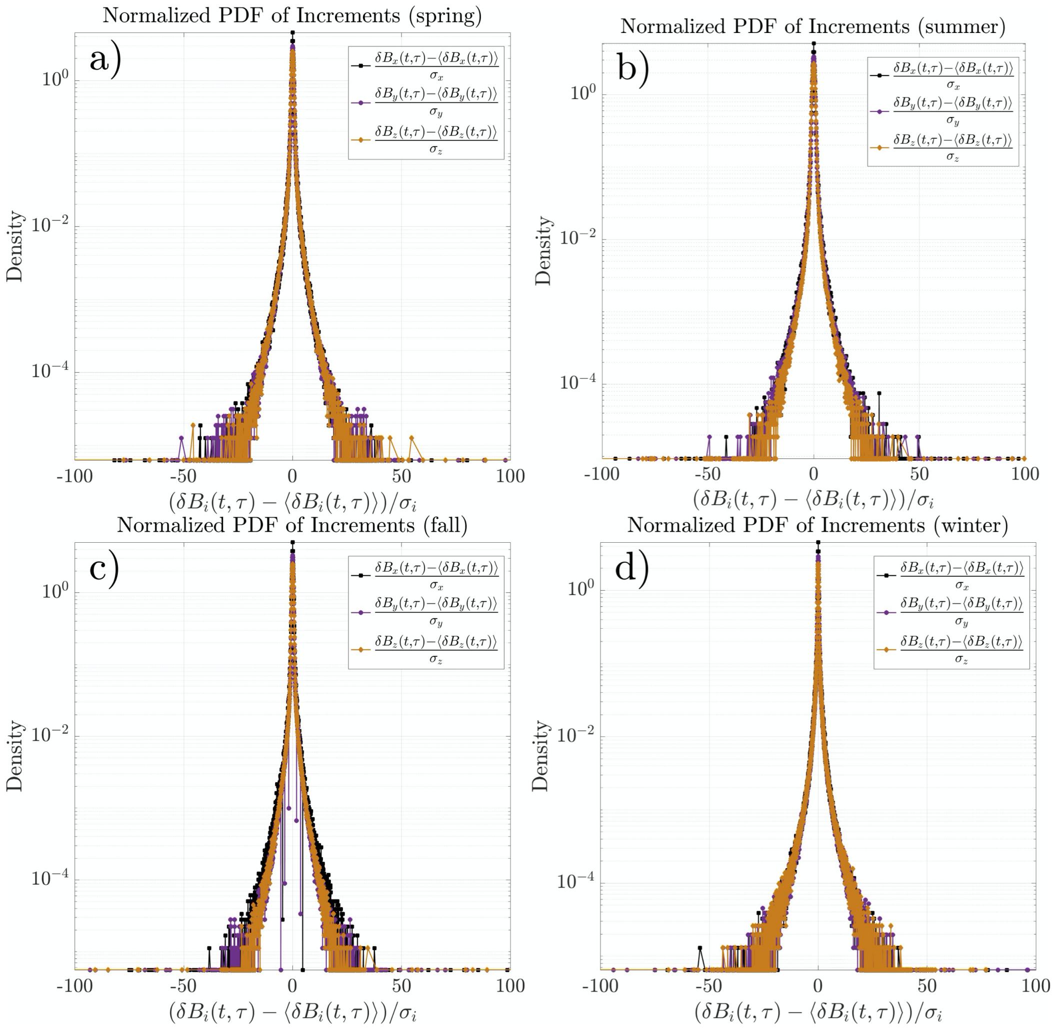

Figure 4. Normalized Probability Distribution Functions (PDF) of increments computed for all upstream solar wind intervals for each Martian season. σ_i represents the standard deviation of $\delta B_i(t,\tau)$.

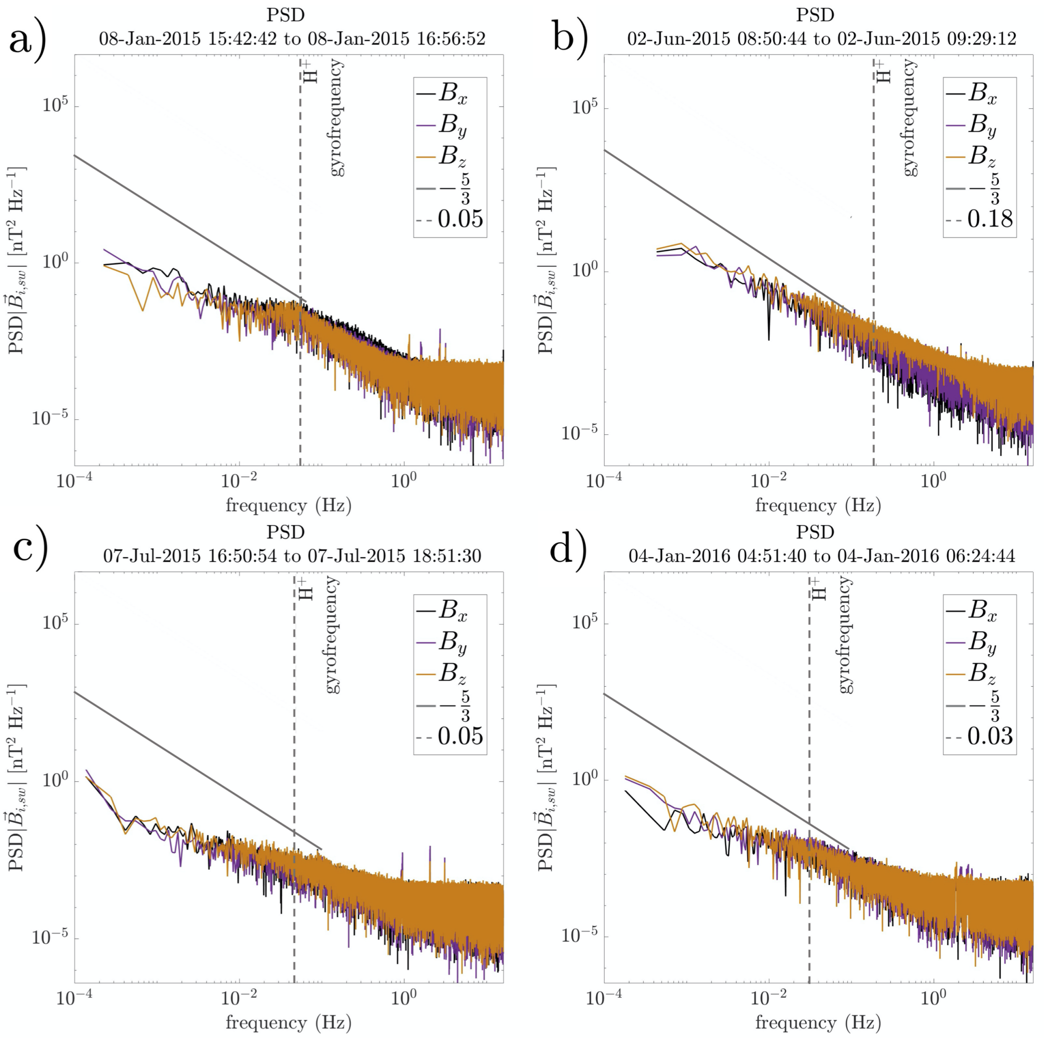

Figure 5. Magnetic Power Spectral Density (PSD) for the longest solar wind interval for each Martian season. Panel (a) corresponds to spring in the southern hemisphere. Panel (b) maps to summer. Panel (c) is taken from fall. Panel (d) corresponds to winter. Included in the PSDs are the -5/3 Kolmogorov spectral index for the inertial range (gray line). The H^+ gyrofrequency for each time interval is plotted as a vertical dashed line.

number of intermittent structures (e.g., Greco et al., 2008, 2009; Salem et al., 2009; Wan et al., 2010). For this study, a τ of 1 was used when computing dB_i.

Figure 5 shows the Power Spectral Densities (PSD) of the magnetic field fluctuations for each Martian season. To compute the PSD of magnetic field fluctuations, the fast Fourier transform (FFT) is calculated for the $\vec{B}_x$, $\vec{B}_y$, and $\vec{B}_z$ components of the magnetic field. As FFTs require uniform sampling (i.e., a time series with no gaps), the FFT of the longest continuous solar wind interval from each season is plotted (see e.g., Munteanu et al. (2016) for the effects of data gaps on spectral analysis). In the study of fluid turbulence, different spatial ranges are considered. Zimbardo et al. (2010) describes the energy containing range, injection scale, inertial range, and dissipation scale that are most used in magnetized plasmas. Only the inertial range is covered in this study. Via different mechanisms (see e.g., Zimbardo et al. (2010)), energy is injected into system, and subsequently transferred to smaller and smaller scales. The transfer is best described by a power-law turbulence spectrum, $E_k \propto k^{-\alpha}$, where E_k is the power spectral density at wavenumber k, and α is the spectral index. The inertial range is between 10^{-4} Hz to 0.1 Hz, and in solar wind, has an α of the Kolmogorov scaling value of -5/3. This line is plotted for reference in gray in Figure 5. The H^+ gyrofrequency calculated for each time interval is plotted as a vertical dashed line.

4 Discussion

This article examines the temperature anisotropy and associated instabilities present around Mars' orbital location. The basic characteristics of magnetic turbulence are also studied in order to compare to known interplanetary solar wind characteristics. The probability distributions of $(\beta_{||p}, R_p)$-values found for January 2015 - December 2016 (Figure 2) closely align to distributions of interplanetary solar wind, such as in Hellinger et al. (2006), and those found in the Earth's magnetosheath such as in Maruca et al. (2018). In all cases, as $\beta_{||p}$ increases, R_p tends toward unity. In Figure 2, there is also a decrease in $\tilde{p}(\beta_{||p}, R_p)$-values near the instability thresholds showing that these instabilities are active. Here, the proton-cyclotron instability is more limiting than the mirror instability for R_p values greater than 1. The same can be said for the summer, fall, and winter seasons for $R_p > 1$ (Figure 3). It is possible that there are also enhanced magnetic fluctuations in the plasma near these thresholds, suggesting that the instabilities are driving the growth of waves. In the case of spring, no definitive assessment is possible due to the corresponding thresholds being so similar at higher $\beta_{||p}$.

The examination of the PDF of magnetic field increments in Figure 4, reveals the appearance of extended tailed PDFs on kinetic scales. The steepening of the spectra suggests dissipation in this range of scales and is consistent with the directly observed heating in the protons. The non-Gaussianity of the PDF of increments for each season shows that there is a presence of intense, phase correlated fluctuations due to the transfer of energy between contiguous eddies. The intermittency observed shows that a nonlinear, non-homogeneous energy transfer is going on.

Examining Figure 5, the spectral indices for the inertial range during summer time periods were found, on average, to be almost exactly the classic Kolmogorov spectral index. This is apparent in the summer PSD plotted in Figure 5 b). Average spectral indices found for solar wind intervals during the Southern hemisphere fall season were also on average closely aligned with the -5/3 slope. This suggests that we did indeed observe mainly solar wind magnetic turbulence. The plasma encountered during this study also exhibits a power spectrum of magnetic field fluctuations characterized by a power law decay. There is evidence of an inertial range with a slope close to -5/3 present in all seasons. Another feature present in approximately 16% of all intervals are peaks and/or bumps around the H^+ gyrofrequency. The majority seen were during the spring (23%) and summer (22%) seasons (e.g., Figure 5 a). Andrés et al. (2020) found that events near the Martian perihelion showed a clear peak in their PSD near the proton cyclotron frequency f_{ci}. The same can be said for this study.

The results of this preliminary study motivate further investigations into how temperature anisotropy constraints arise in Martian exosphere and how they impact the large-scale evolution of the plasma. More numerous and lengthy time periods are needed to decouple the impact of the Martian exosphere on R_p values. Endeavors to determine systematic differences in temperature anisotropy that can be accounted for by seasonal variability would also be of interest. As MAVEN and other Mars-orbiting spacecraft continue to return valuable observations, queries regarding the properties of turbulence and plasma instabilities upstream of Mars can be resolved.

Acknowledgments

The MAVEN mission has been made possible through NASA sponsorship and the dedicated efforts of NASA Goddard Space Flight Center, LASP, Lockheed Martin, and the MAVEN Technical and Science Teams. The MAVEN data shown are publicly available at the NASA Planetary Data System website (http://ppi.pds.nasa.gov).

References

Andrés, N., Romanelli, N., Hadid, L. Z., Sahraoui, F., DiBraccio, G., & Halekas, J. (2020). Solar wind turbulence around mars: Relation between the energy cascade rate and the proton cyclotron waves activity. *The Astrophysical Journal*, *902*, 134 - 143. doi: https://doi.org/10.3847/1538-4357/abb5a7

Bhattacharyya, D., Clarke, J. T., Chaufray, J. Y., Mayyasi, M., Bertaux, J. L., Chaffin, M. S., … Villanueva, G. L. (2017). Seasonal changes in hydrogen escape from mars through analysis of hst observations of the martian exosphere near perihelion. *Journal of Geophysical Research: Space Physics*, *122*(11), 11,756-11,764. doi: https://doi.org/10.1002/2017JA024572

Bruno, R., & Carbone, V. (2016). *Turbulence in the solar wind.* Springer. doi: 10.1007/978-3-319-43440-7

Connerney, J. E. P., Espley, J., Lawton, P., Murphy, S., Odom, J., Oliversen, R., & Sheppard, D. (2015). The maven magnetic field investigation. *Space Science Reviews*, *195*, 257–291. doi: 10.1007/s11214-015-0169-4

Espley, J. R. (2018). The martian magnetosphere: Areas of unsettled terminology. *Journal of Geophysical Research: Space Physics*, *123*(6), 4521–4525. doi: 10.1029/2018JA025278

Greco, A., Chuychai, P., Matthaeus, W. H., Servidio, S., & Dmitruk, P. (2008). Intermittent mhd structures and classical discontinuities. *Geophysical Research Letters*, *35*(19). doi: https://doi.org/10.1029/2008GL035454

Greco, A., Matthaeus, W. H., Servidio, S., Chuychai, P., & Dmitruk, P. (2009). Statistical analysis of discontinuities in solar wind ace data and comparison with intermittent mhd turbulence. *The Astrophysical Journal*, *691*(2), L111–L114. doi: 10.1088/0004-637x/691/2/l111

Halekas, J. S. (2017). Seasonal variability of the hydrogen exosphere of mars. *Journal of Geophysical Research: Planets*, *122*, 901–911. doi: doi:10.1002/2017JE005306

Halekas, J. S., Ruhunusiri, S., Harada, Y., Collinson, G., Mitchell, D. L., Mazelle, C., … Jakosky, B. M. (2017). Structure, dynamics, and seasonal variability of the mars-solar wind interaction: Maven solar wind ion analyzer in-flight performance and science results. *Journal of Geophysical Research: Space Physics*, *122*(1), 547-578. doi: https://doi.org/10.1002/2016JA023167

Halekas, J. S., Taylor, E. R., Dalton, G., Johnson, G., Curtis, D. W., McFadden, J. P., … Jakosky, B. M. (2015). The solar wind ion analyzer for maven. *Space Science Reviews*, *195*, 125-151. doi: 10.1007/s11214-013-0029-z

Hellinger, P., Trávníček, P., Kasper, J. C., & Lazarus, A. J. (2006). Solar wind proton temperature anisotropy: Linear theory and wind/swe observations. *Geophysical Research Letters*, *33*(9). doi: https://doi.org/10.1029/2006GL025925

Horbury, T. S., Forman, M., & Oughton, S. (2008, Oct). Anisotropic scaling of magnetohydrodynamic turbulence. *Phys. Rev. Lett.*, *101*, 175005. doi: 10.1103/PhysRevLett.101.175005

Howes, G. G. (2008). Inertial range turbulence in kinetic plasmas. *Physics of Plasmas*, *15*(5), 055904. doi: 10.1063/1.2889005

Klein, K. G., & Howes, G. G. (2015). Predicted impacts of proton temperature anisotropy on solar wind turbulence. *Physics of Plasmas*, *22*(3), 032903. doi: 10.1063/1.4914933

Kolmogorov, A. (1941, January). The Local Structure of Turbulence in Incompressible Viscous Fluid for Very Large Reynolds' Numbers. *Akademiia Nauk SSSR Doklady*, *30*, 301-305.

Kolmogorov, A. N. (1941, April). Dissipation of Energy in Locally Isotropic Turbulence. *Akademiia Nauk SSSR Doklady*, *32*, 16.

Luhmann, J. (1992). Comparative studies of the solar wind interaction with weakly magnetized planets. *Advances in Space Research*, *12*(9), 191 - 203. doi: https://doi.org/10.1016/0273-1177(92)90331-Q

Marsch, E., & Tu, C.-Y. (1997). Intermittency, non-gaussian statistics and fractal scaling of mhd fluctuations in the solar wind. *Nonlinear Processes in Geophysics*, *4*(2), 101–124. doi: 10.5194/npg-4-101-1997

Maruca, B. A., Chasapis, A., Gary, S. P., Bandyopadhyay, R., Chhiber, R., Parashar, T. N., ... Strangeway, R. J. (2018). Mms observations of beta-dependent constraints on ion temperature anisotropy in earth's magnetosheath. *The Astrophysical Journal*, *866*, 25-30. doi: https://doi.org/10.3847/1538-4357/aaddfb

Maruca, B. A., Kasper, J. C., & Bale, S. D. (2011). What are the relative roles of heating and cooling in generating solar wind temperature anisotropies? *Physical Review Letters*, *107*, 201101. doi: 10.1103/PhysRevLett.107.201101

Maruca, B. A., Kasper, J. C., & Gary, S. P. (2012). Instability-driven limits on helium temperature anisotropy in the solar wind: Observations and linear vlasov analysis. *The Astrophysical Journal*, *748*, 137-143. doi: 10.1088/0004-637X/748/2/137

Matteini, L., Landi, S., Hellinger, P., Pantellini, F., Maksimovic, M., Velli, M., ... Marsch, E. (2007). Evolution of the solar wind proton temperature anisotropy from 0.3 to 2.5 au. *Geophysical Research Letters*, *34*(20). doi: https://doi.org/10.1029/2007GL030920

Matthaeus, W. H., & Goldstein, M. L. (1982). Measurement of the rugged invariants of magnetohydrodynamic turbulence in the solar wind. *Journal of Geophysical Research*, *87*(A8), 6011-6028. doi: https://doi.org/10.1029/JA087iA08p06011

Mazelle, D. S. K., C.and Winterhalter, Trotignon, J., Acuña, M., Baumgärtel, K., Bertucci, C., Brain, D., ... Slavin, J. (2004). Bow shock and upstream phenomena at mars. *Space Science Reviews*, *111*, 115-181. doi: https://doi.org/10.1023/B:SPAC.0000032717.98679.d0

Munteanu, C., Negrea, C., Echim, M., & Mursula, K. (2016). Effect of data gaps: comparison of different spectral analysis methods. *Annales Geophysicae*, *34*(4), 437–449. doi: 10.5194/angeo-34-437-2016

Osman, K. T., Matthaeus, W. H., Gosling, J. T., Greco, A., Servidio, S., Hnat, B., ... Phan, T. D. (2014). Magnetic reconnection and intermittent turbulence in the solar wind. *Physical Review Letters*, *112*, 215002-215007. doi: 10.1103/PhysRevLett.112.215002

Osman, K. T., Matthaeus, W. H., Hnat, B., & Chapman, S. C. (2012). Kinetic signatures and intermittent turbulence in the solar wind plasma. *Physical Review Letters*, *108*, 261103-261107. doi: 10.1103/PhysRevLett.108.261103

Parashar, T. N., Salem, C., Wicks, R. T., Karimabadi, H., Gary, S. P., & Matthaeus, W. H. (2015). Turbulent dissipation challenge: a community-driven effort. *Journal of Plasma Physics*, *81*(5), 905810513. doi: 10.1017/S0022377815000860

Pine, Z. B., Smith, C. W., Hollick, S. J., Argall, M. R., Vasquez, B. J., Isenberg, P. A., ... McLaurin, M. L. (2020). Solar wind turbulence from 1 to 45 au. iv. turbulent transport and heating of the solar wind using voyager observations. *The Astrophysical Journal*, *900*(2), 91-102. doi: https://doi.org/10.3847/1538-4357/abab12

Ruhunusiri, S., Halekas, J. S., Espley, J. R., Mazelle, C., Brain, D., Harada, Y., ... Howes, G. G. (2017). Characterization of turbulence in the mars plasma environment with maven observations. *Journal of Geophysical Research: Space*

Physics, *122*(1), 656-674. doi: https://doi.org/10.1002/2016JA023456

Salem, C., Mangeney, A., Bale, S. D., & Veltri, P. (2009). Solar wind magnetohydrodynamics turbulence: anomalous scaling and role of intermittency. *The Astrophysical Journal*, *702*(1), 537–553. doi: 10.1088/0004-637x/702/1/537

Slavin, J. A., & Holzer, R. E. (1981). Solar wind flow about the terrestrial planets 1. modeling bow shock position and shape. *Journal of Geophysical Research*, *86*(A13), 11401-11418. doi: https://doi.org/10.1029/JA086iA13p11401

Sorriso-Valvo, L., Carbone, V., Veltri, P., Consolini, G., & Bruno, R. (1999). Intermittency in the solar wind turbulence through probability distribution functions of fluctuations. *Geophysical Research Letters*, *26*(13), 1801-1804. doi: https://doi.org/10.1029/1999GL900270

Verscharen, D., Klein, K. G., & Maruca, B. A. (2019). The multi-scale nature of the solar wind. *Living Reviews in Solar Physics*, *16*(5). doi: https://doi.org/10.1007/s41116-019-0021-0

Wan, M., Oughton, S., Servidio, S., & Matthaeus, W. H. (2010). On the accuracy of simulations of turbulence. *Physics of Plasmas*, *17*(8), 082308. doi: 10.1063/1.3474957

Zimbardo, G., Greco, A., Sorriso-Valvo, L., Perri, S., Vörös, Z., Aburjania, G., … Alexandrova, O. (2010). Magnetic turbulence in the geospace environment. *Space Science Reviews*, *156*, 89-134. doi: 10.1007/s11214-010-9692-5

On the Solar Wind Proton Temperature Anisotropy at Mars' Orbital Location

C. L. Lentz[1], A. Chasapis[1], R. A. Qudsi[2], J. Halekas[3], B. A. Maruca[2], L. Andersson[1], D. N. Baker[1]

[1]Laboratory for Atmospheric and Space Physics, University of Colorado, Boulder, CO, USA
[2]Department of Physics and Astronomy, University of Delaware, Newark, DE, USA
[3]Department of Physics and Astronomy, University of Iowa, Iowa City, IA, USA

Key Points:

- Microinstabilities play a role in limiting proton temperature anisotropy (both $\frac{T_{\perp p}}{T_{||p}} > 1$ and $\frac{T_{\perp p}}{T_{||p}} < 1$) upstream of Mars
- Probability Density Functions of magnetic field fluctuations exhibit intermittent structures present in upstream plasma at Mars
- Power Spectral Densities of magnetic field fluctuations demonstrate an inertial range with Kolmogorov scaling value of -5/3

Corresponding author: C. L. Lentz, `christy.lentz@lasp.colorado.edu`

Abstract

The Mars Atmosphere and Volatile EvolutionN (MAVEN) spacecraft can act as an intermittent upstream solar wind monitor at ~ 1.5 AU. To inspect the evolution of solar wind turbulence in the Martian exosphere, we have gathered proton (i.e., ionized hydrogen) temperature measurements taken by the Solar Wind Ion Analyzer (SWIA) onboard the MAVEN spacecraft. Here we investigate instabilities driven by the proton temperature anisotropy at Mars. We look at the temperature anisotropy $T_{\perp p}/T_{||p}$ (i.e., the ratio of the perpendicular proton temperature component to the parallel proton temperature component) and the parallel plasma beta, $\beta_{||p}$, to determine the active plasma instability mode. Furthermore, we report on the properties of turbulence near Mars' orbital location during upstream solar wind intervals from January 2015 to December 2016 (~ 1 Martian year). We find that the probability distributions of $(\beta_{||p}, R_p)$-values are limited at $R_p > 1$ and $R_p < 1$. We also find evidence of intermittency implying non-linear, non-homogeneous energy transfer. Additionally, spectral index values near the Kolmogorov scaling value are observed for the inertial range (10^{-4} Hz to 0.1 Hz).

Plain Language Summary

Radially emanating from the Sun, solar wind consists of highly ionized and strongly magnetized plasma. During its expansion, the solar wind develops into a turbulent flow. With increasing distance from the Sun, based on the thermodynamic adiabatic expansion law, one would expect the temperature of protons in the solar wind to decrease at a certain rate. Instead we see that protons are hotter than expected; and therefore some heating mechanism must be at work. Due to the fact that turbulence functions as a reservoir of energy, instabilities associated with turbulent flows can then disperse free energy by wave excitation; subsequently heating the plasma. For idealized situations, the local free energy content of the solar wind can be characterized by the proton temperature anisotropy. While there have been multiple spacecraft to characterize turbulence and proton temperature anisotropies at 1 AU, there exist limited opportunities to obtain these same measurements beyond this orbital location. To study the basic properties of turbulence and proton temperature anisotropies at Mars' orbital location, we used the Mars Atmosphere and Volatile EvolutionN (MAVEN) spacecraft.

1 Introduction

1.1 Turbulence in the Solar Wind

Solar wind is a supersonic and super Alfvénic plasma flow originating from the Sun. It is a continuously expanding plasma that is highly ionized and threaded with large scale magnetic fields (Bruno & Carbone, 2016). The thermodynamic adiabatic expansion law applied to proton temperatures in the solar wind would suggest that temperature declines with heliocentric distance as $T(r) \sim r^{-\frac{4}{3}}$. However, this is not the case, and solar wind evolves in a highly non-trivial way as it expands from the Sun (e.g., Matteini et al., 2007). There exist numerous observations to imply that some heating mechanism must be at work within the solar wind to supply the energy required to slow down the decay (Pine et al., 2020).

One potential explanation for this heating is turbulence. As the highly ionized and magnetized solar wind develops into a turbulent flow at large scales, it can act as a reservoir of energy. As eddies in the turbulent plasma interact, they break up into smaller eddies, undergoing what is known as an energy cascade. In this energy cascade, there is a net transfer of energy from large scales, where turbulence first develops, to small scales, where dissipative mechanisms convert turbulent energy to heat (Verscharen et al., 2019; Bruno & Carbone, 2016; Howes, 2008; Klein & Howes, 2015).

The turbulent effects of the plasma can be described in a magnetohydrodynamic (MHD) framework (Matthaeus & Goldstein, 1982). This flow can also be described by hydrodynamic turbulence described by Kolmogorov at low frequency and long wavelengths (A. N. Kolmogorov, 1941; A. Kolmogorov, 1941). Plasma instabilities and associated wave particle interactions play a role in all observations at 1 AU. However, studies of solar wind turbulence outside of 1 AU are limited by instrument capabilities. The exception being the Ulysses spacecraft (1990-2009), whose magnetic field observations were used to study anisotropies of the solar wind turbulence at 1.4 AU from the Sun (Horbury et al., 2008).

To inspect the evolution of solar wind turbulence and proton temperature anisotropies in and upstream of the Martian atmosphere, we have gathered magnetic field data (MAG; Connerney et al., 2015) and proton temperature measurements taken by the Solar Wind Ion Analyzer (SWIA; Halekas et al., 2015) both onboard the MAVEN spacecraft. Here we examine Probability Distribution Functions (PDFs) and Power Spectral Densities (PSDs) of magnetic field fluctuations to report on solar wind turbulence near Mars' orbital location. Furthermore, we investigate instabilities driven by the proton temperature anisotropy at Mars to determine the plasma instability modes most active. These results provide novel insights into the physics of solar wind around Mars and contribute to the understanding of the role turbulence and plasma instabilities play in the evolution of the solar wind.

1.2 The Martian Plasma Environment

Mars acts as an obstacle to the supersonic and magnetized plasma emanating from the Sun. A shock wave is formed in front of the planet known as the bow shock. It serves to slow down the flowing solar wind from supersonic to subsonic speeds (Luhmann, 1992; Mazelle et al., 2004). Plasma thermalization then occurs in the sheath, at and downstream of the shock (Luhmann, 1992).

One fascinating feature of Mars is an exosphere that extends beyond the bow shock due to the weaker gravity of the planet (Mazelle et al., 2004). Above the exobase (altitude $\sim$ 200 km; Bhattacharyya et al., 2017) an extended exosphere is formed in part due to the ballistic motion of hydrogen atoms (Anderson, 1974; Anderson and Hord, 1971; Chaufray et al., 2008; Feldman et al., 2011; Chaffin et al., 2015). There is known to be a high degree of variability of the hydrogen density of the exosphere, with peak hydrogen densities occurring at Solar Longitude (L_s) values $\sim$ 263-288°, roughly centered on Mars southern summer solstice ($L_s = 270°$; Halekas, 2017). Where L_s is the Mars-Sun angle measured from the Northern Hemisphere spring equinox ($L_s = 0°$). This causes the solar wind/Mars interaction and therefore upstream dynamics at Mars to be very complex.

Further differences between plasma properties at Earth and Mars arise from Mars' greater heliocentric distance and its smaller size. The lower solar wind density and interplanetary magnetic field (IMF) strength makes for a different Mach number. Due to the smaller planet size and diminished IMF strength, the gyroradius of solar wind protons is comparable to the size of the shock, making kinetic effects important (Mazelle et al., 2004).

Few studies have investigated turbulence at Mars. Ruhunusiri et al. (2017) was the first known study to characterize turbulence in the Mars plasma environment. They determined that turbulence characteristics at Mars vary seasonally. Additionally, they found that a fully developed energy cascade is absent in the magnetosheath of Mars, but present in the magnetic pileup boundary (also known as the induced magnetosphere boundary; see Espley (2018) for a debate on the nomenclature). A study conducted by Andrés et al. (2020) estimated the incompressible energy cascade rate at MHD scales in the plasma upstream of the bow shock for events with and without proton cyclotron wave (PCW) activity. To date, there have been no known studies looking into the proton temperature anisotropy at Mars, and therefore this article aims to provide an evaluation of temperature anisotropy instabilities.

2 Methodology

2.1 Data

In order to analyze plasma instabilities and associated wave-particle interactions at Mars' orbital location, we used SWIA to obtain 3D distributions of proton temperature moments. SWIA is an electrostatic analyzer designed to measure solar wind and magnetospheric ions in the Martian planetary environment. Among other quantities, temperature is calculated on board from SWIA coarse data when MAVEN is in the sheath, or fine data when MAVEN is in its solar wind mode. A few caveats of note are that moments are computed assuming the entire distribution is within the field of view and energy range of SWIA. Also, the assumption that all ions are protons is made which can be problematic when looking into the data quantitatively. The upstream solar wind consists of $\sim$ 94-97% protons and $\sim$ 3-6% alpha particles. Any alpha particles present in the distribution, which SWIA is using to compute the temperature moment, can lead to artificially large values. This effect is most prominent in the component of the temperature moment that is aligned with the flow. Another potential hiccup arises when attempting to completely resolve temperatures when cold plasma beams are being sampled. This is due to the $\sim$ 15% energy resolution of SWIA. Not all hope is lost however, as proton temperatures can be calculated by taking SWIA level 2 3D fine data and separately computing proton and alpha temperature moments using a routine discussed in (Halekas et al., 2017).

Alpha particles are typically separated along the magnetic field from the protons. By locating proton and alpha peaks in the 3D distributions, the energy in between them can be bisected. Everything on the alpha side of the break is then disregarded, and the proton moments are then calculated. When thermal velocity is small compared to bulk velocity, alpha particles show up at twice the energy per charge than protons, and therefore can be separated. This is challenging to do so with really hot distributions, as SWIA does not have mass resolution capabilities. This causes difficulty in discerning proton and alpha peaks because they overlap in hot distributions. Besides these caveats, the routine successfully generates x, y, and z components of proton temperatures in magnetic field aligned coordinates. The z component is then $T_{||p}$, or the parallel proton temperature component. The average of x and y components is taken to be $T_{\perp p}$, or the perpendicular temperature component.

MAG measurements were used to calculate the parallel plasma beta component, $\beta_{||p}$, and to facilitate solar wind interval identification. Two tri-axial fluxgate magnetometer sensors measure the vector magnetic field throughout the Martian plasma environment over a wide dynamic range with a resolution up to 0.008 nT at an accuracy of around 0.05%. The better of the two magnetometers are used to sample the ambient magnetic field at a rate of 32 vector samples per second and create the standard data product.

Although it is debatable if MAVEN's orbit ever encounters truly pristine upstream solar wind at Mars due to the exosphere, there is still plenty of information that can be gleaned about turbulence and temperature anisotropies. An example of a manually identified upstream solar wind period on January 9th 2015 using SWIA and MAG measurements is shown in Figure 1. Panel a) displays the x, y, and z position coordinates of MAVEN, along with the altitude in units of Mars radii using the Mars-Sun-Orbital (MSO) coordinate system (see Slavin and Holzer (1981) page 11,404 for a detailed explanation on MSO coordinate system). Panel b) shows the magnetic field vector measurements in MSO coordinates ($\vec{B}_x$, $\vec{B}_y$, and $\vec{B}_z$), the magnitude of the magnetic field ($|\vec{B}_{sw}|$), and the inverse of the magnitude of the magnetic field($-|\vec{B}_{sw}|$). Panel c) shows SWIA measured

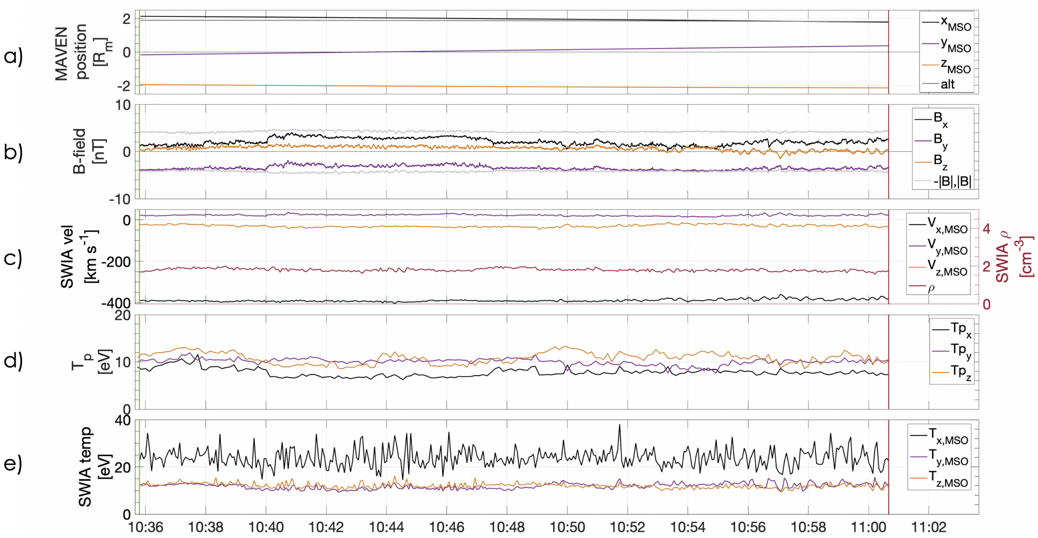

Figure 1. A solar wind interval manually identified from January 9, 2015. Panel a) shows MAVEN position in MSO coordinates in units of Mars radii obtained from key parameters data set. Panel b) shows the magnitude of the magnetic field, $|B|$, inverse $|B|$, the Bx, By, and Bz components in MSO coordinates. Panel c) shows SWIA velocity component measurements in MSO coordinates (left axis), and SWIA density measurements (right axis). Panel d) shows calculated proton temperature measurements. Panel e) onboard SWIA temperature moments.

MSO velocity coordinates on the left axis, and ion density measurements on the right axis. Panel d) shows the computed proton temperature measurements. Panel e) shows the SWIA temperature moments calculated onboard.

Upstream solar wind intervals were identified for the 1st through the 10th of each month from January 2015 to December 2016. The number of intervals each month were limited by the availability of the proton temperature moments. Upstream solar wind periods at Mars were recognized in the magnetic field by diminished fluctuations in the magnetic field components, and low vector magnitude ($|\vec{B}_{sw}| \leq 10$ nT) compared to other plasma regions and boundaries. Also, the typical density rose no higher than 10 protons per cubic centimeter ($\rho \leq 10$ cm^{-3}). There was also a steady negative x component of the velocity ($\vec{V}_x < 0$).

From these intervals turbulent statistics and temperature anisotropies were then calculated. To access the start and stop times along with maxima, minima, medians, and averages of every parameter discussed in this study, please reference the supplementary material. The solar wind intervals were then classified into southern hemisphere Martian seasons using the L_s values. $0 < L_s < 89°$ represents the Martian fall season, $90 < L_s < 179°$ corresponds to winter, $180 < L_s < 269°$ corresponds to spring, and $270 < L_s < 359°$ corresponds to summer. For this study, 2015-07-01 to 2016-01-03/02:22:08 corresponded to autumn. Winter months were 2016-01-03/02:22:16 - 2016-07-04/15:39:44. Spring mapped to the time periods 2015-01 and from 2016-07-04/15:39:52 to 2016-11. Summer months were from 2015-02 to 2015-06, and 2016-12.

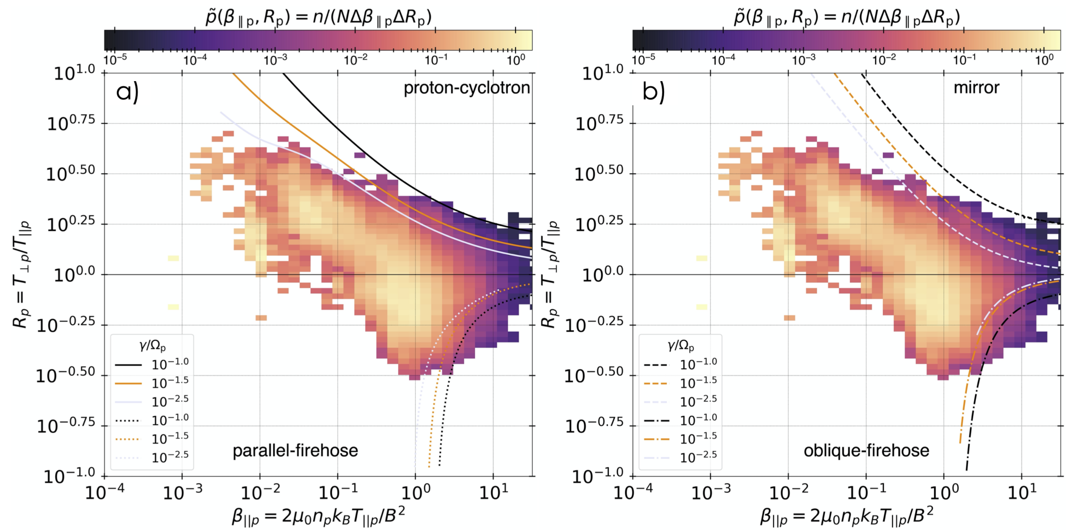

Figure 2. Probability distributions of $(\beta_{||p}, R_p)$-values from January 2015 to December 2016. a) depicts probability distributions with contours of constant growth rate (in units of proton cyclotron frequency $[\Omega_p]$) for parallel instabilities. The solid lines in the upper right corner of a) represent constant growth rates for the proton-cyclotron instability, while the dotted lines represent the parallel-firehose instability. The dashed lines in b) show the mirror instability, while the dot-dashed lines show the oblique-firehose instability.

3 Results

3.1 Probability distributions of $(\beta_{||p}, R_p)$-values

Due to the solar wind's strong magnetic field, the transport of energy is direction dependent, which can bring about temperature anisotropy. The temperature anisotropy in protons can be described by the following ratio.

$$R_p = \frac{T_{\perp p}}{T_{||p}} \tag{1}$$

Where R_p is the ratio of the proton temperature component perpendicular to the local mean magnetic field ($T_{\perp p}$), to the proton temperature component parallel to the magnetic field ($T_{||p}$). The distribution of R_p values observed in the solar wind depend strongly on the ratio of the parallel proton pressure to the magnetic pressure, known as the parallel plasma beta (Maruca et al., 2018).

$$\beta_{||p} = \frac{n_p k_B T_{||p}}{|\vec{B}_{sw}|^2/(2\mu_0)} \tag{2}$$

Where n_p is the proton density, k_B is the Boltzmann constant, and μ_0 is the vacuum permeability.

A R_p value of 1 corresponds to temperature isotropy (i.e., a state of equilibrium). If R_p deviates from unity, proton temperature anisotropy may prompt various plasma instabilities. Some commonly known instabilities such as the proton-cyclotron instability and/or the mirror instability arise when the perpendicular proton temperature component is larger than the parallel proton temperature component ($T_{\perp p} > T_{||p}$). However, when the parallel proton temperature component is larger than the perpendicu-

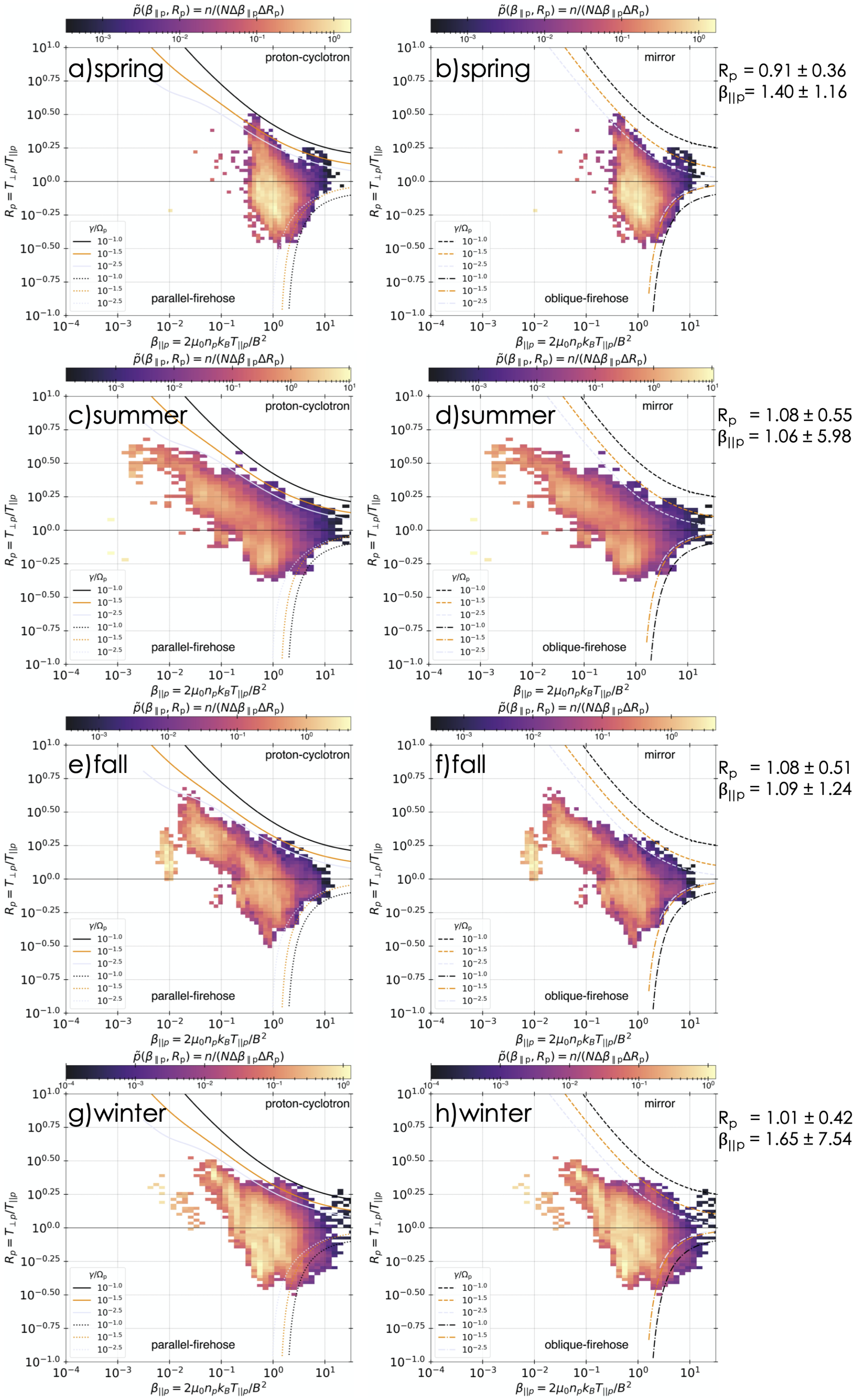

Figure 3. Probability distributions of $(\beta_{||p}, R_p)$-values for each Martian southern hemisphere season examined. a), c), e), and g) display probability distributions for parallel instabilities for spring, summer, fall and winter. b), d), f), and h) display probability distributions for perpendicular instabilities for spring, summer, fall and winter. Included to the right of all plots are the average plus/minus the standard deviation of R_p and $\beta_{||p}$.

lar proton temperature component ($T_{||p} > T_{\perp p}$), the parallel and/or the oblique firehose instabilities may arise.

To search for the effects of various instabilities, the approach outlined in Maruca et al. (2018) was used to plot the distribution of observations over the $(\beta_{||p}, R_p)$-plane using equations 1 and 2. The $(\beta_{||p}, R_p)$-plane is a tool to study the impact of anisotropy-driven instabilities on protons in the solar wind.

Figure 2 displays the probability distributions of $(\beta_{||p}, R_p)$-values $[\tilde{p}(\beta_{||p}, R_p)]$ for the entire study. Figure 3 displays $\tilde{p}(\beta_{||p}, R_p)$ for each season. The average $\pm$ the standard deviation of R_p and $\beta_{||p}$ are also displayed to the right of each season. The overlaid curves in both figures show the contours of constant growth rate (γ) for different instabilities, normalized by the proton frequency (Ω_p). Following the method originally outlined in Maruca et al. (2011), the growth rate of an instability is taken to be the growth rate of its fastest-growing wave mode. An instability is defined as being active if some wave modes are growing ($\gamma > 0$). Growth rates of anisotropy-driven instabilities are dependent upon $\beta_{||p}$ and R_p values. Therefore a common analysis technique is to plot contours of constant γ in the $(\beta_{||p}, R_p)$-plane. $\gamma(\beta_{||p}, R_p)$ is taken to be the growth rate of the fastest-growing mode for that set of values and is normalized to the proton frequency, $\Omega_p = q_p B/m_p$, where q_p is the charge and m_p is the mass of a proton. All of these contours were calculated using the linear Vlasov software described by Maruca et al. (2012), which considers an idealized plasma where each population of particles has a biMaxwellian velocity distribution function. For the present study, electrons were assumed to be isotropic. Likewise, the presence of proton beams and α-particles was neglected.

3.2 Turbulence at Mars

The study of temperature anisotropy in conjunction with turbulence at Mars' orbital location was motivated by such studies as Osman et al. (2012, 2014). The authors provided evidence that a turbulent cascade from inertial to kinetic scales is the causal agent allowing the solar wind to populate the extremes of the $(\beta_{||p}, R_p)$-plane. They suggested that while instabilities may act to confine the solar wind plasma, turbulent fluctuations and cascade rates can cause temperature anisotropies, intermittent structures, and heating in the $(\beta_{||p}, R_p)$-plane.

Intermittent structures are a feature of turbulence. One way to quantify intermittency of turbulence is to calculate the probability distribution function (PDF). PDFs of turbulent quantities are Gaussian, but the PDFs of increments of a turbulent quantity are not. By taking the increments of the magnetic field components ($\delta B_i(t, \tau) = B_i(t) - B_i(t+\tau)$), we can highlight the gradients or high magnetic stress and coherent structures (Osman et al., 2012), and hence the intermittent structures present (Parashar et al., 2015; Sorriso-Valvo et al., 1999). Observations of intermittency imply that a non-linear, non-homogeneous energy transfer is going on. Here the subscript i represents the x, y, or z magnetic field component, and τ represents the lag. Figure 4 displays the normalized PDFs of magnetic field fluctuations for each Martian season. Each PDF of increments is normalized using $(\delta B_i(t, \tau) - \langle \delta B_i(t, \tau) \rangle)/\sigma_i$ where σ_i represents the standard deviation of $\delta B_i(t, \tau)$. Intermittency is highlighted by heavy tails in the PDFs of increments, and is present in all four seasons.

The solar wind is a highly variable environment, and extreme values of increments can be present, such as the tails shown throughout Figure 4. The inertial range solar wind PDF is known to have a typical shape with a narrow peak and fat tails (Marsch & Tu, 1997). The strength of the gradients highlighted depends on the lag τ. Smaller values of τ help highlight gradients (i.e., intermittent structures). When τ becomes comparable to the correlation length of the system, the PDFs revert back to Gaussianity. It has been shown that the non-Gaussian tails on the PDFs of increments correspond to the

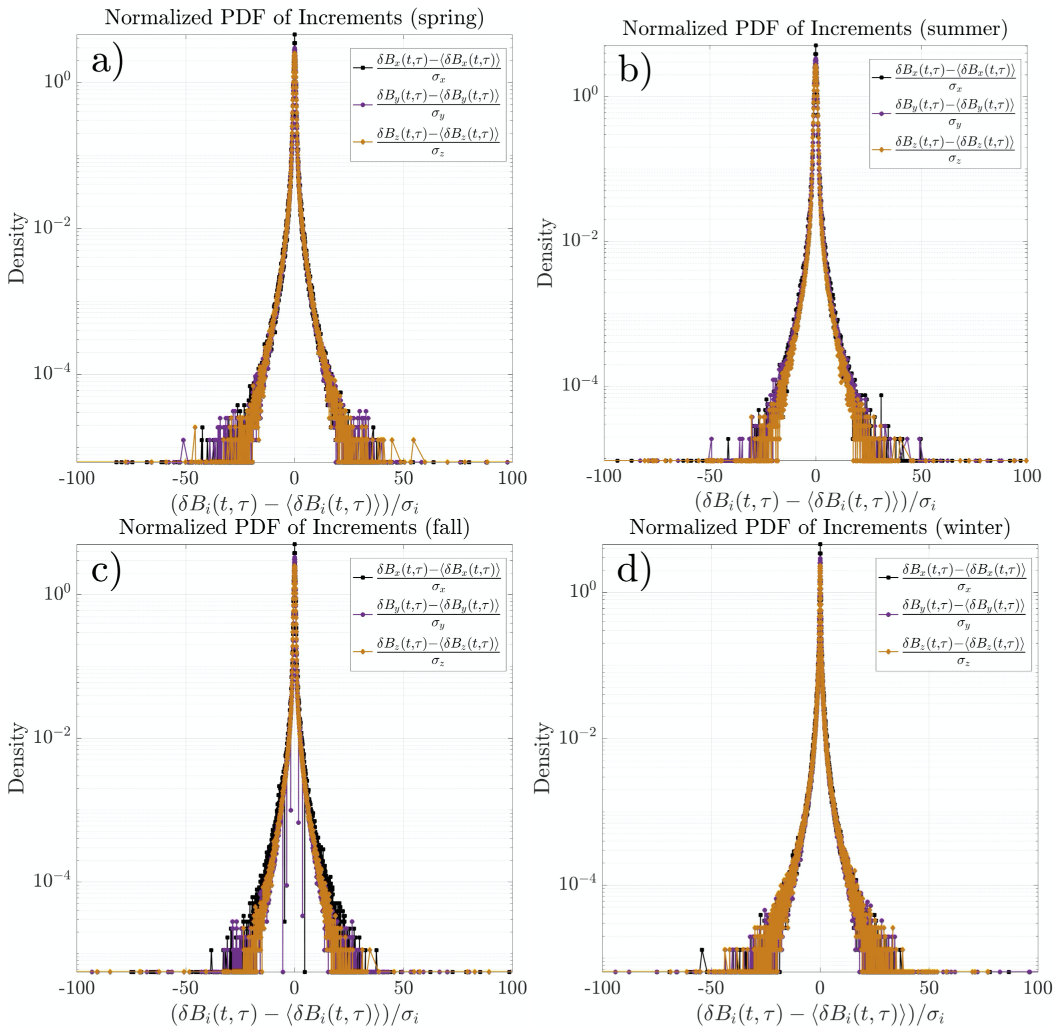

Figure 4. Normalized Probability Distribution Functions (PDF) of increments computed for all upstream solar wind intervals for each Martian season. σ_i represents the standard deviation of $\delta B_i(t,\tau)$.

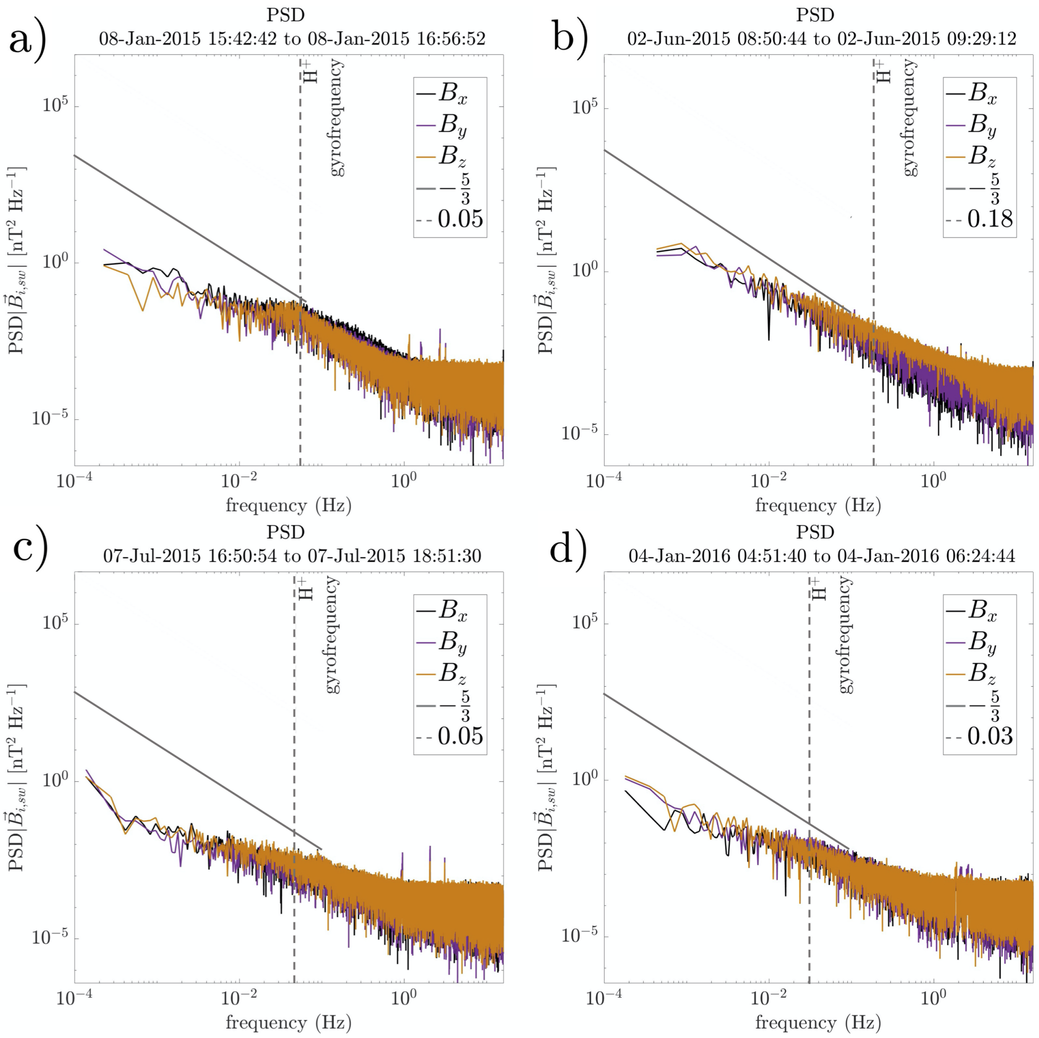

Figure 5. Magnetic Power Spectral Density (PSD) for the longest solar wind interval for each Martian season. Panel (a) corresponds to spring in the southern hemisphere. Panel (b) maps to summer. Panel (c) is taken from fall. Panel (d) corresponds to winter. Included in the PSDs are the -5/3 Kolmogorov spectral index for the inertial range (gray line). The H^+ gyrofrequency for each time interval is plotted as a vertical dashed line.

number of intermittent structures (e.g., Greco et al., 2008, 2009; Salem et al., 2009; Wan et al., 2010). For this study, a τ of 1 was used when computing dB_i.

Figure 5 shows the Power Spectral Densities (PSD) of the magnetic field fluctuations for each Martian season. To compute the PSD of magnetic field fluctuations, the fast Fourier transform (FFT) is calculated for the $\vec{B}_x$, $\vec{B}_y$, and $\vec{B}_z$ components of the magnetic field. As FFTs require uniform sampling (i.e., a time series with no gaps), the FFT of the longest continuous solar wind interval from each season is plotted (see e.g., Munteanu et al. (2016) for the effects of data gaps on spectral analysis). In the study of fluid turbulence, different spatial ranges are considered. Zimbardo et al. (2010) describes the energy containing range, injection scale, inertial range, and dissipation scale that are most used in magnetized plasmas. Only the inertial range is covered in this study. Via different mechanisms (see e.g., Zimbardo et al. (2010)), energy is injected into system, and subsequently transferred to smaller and smaller scales. The transfer is best described by a power-law turbulence spectrum, $E_k \propto k^{-\alpha}$, where E_k is the power spectral density at wavenumber k, and α is the spectral index. The inertial range is between 10^{-4} Hz to 0.1 Hz, and in solar wind, has an α of the Kolmogorov scaling value of -5/3. This line is plotted for reference in gray in Figure 5. The H^+ gyrofrequency calculated for each time interval is plotted as a vertical dashed line.

4 Discussion

This article examines the temperature anisotropy and associated instabilities present around Mars' orbital location. The basic characteristics of magnetic turbulence are also studied in order to compare to known interplanetary solar wind characteristics. The probability distributions of $(\beta_{||p}, R_p)$-values found for January 2015 - December 2016 (Figure 2) closely align to distributions of interplanetary solar wind, such as in Hellinger et al. (2006), and those found in the Earth's magnetosheath such as in Maruca et al. (2018). In all cases, as $\beta_{||p}$ increases, R_p tends toward unity. In Figure 2, there is also a decrease in $\tilde{p}(\beta_{||p}, R_p)$-values near the instability thresholds showing that these instabilities are active. Here, the proton-cyclotron instability is more limiting than the mirror instability for R_p values greater than 1. The same can be said for the summer, fall, and winter seasons for $R_p > 1$ (Figure 3). It is possible that there are also enhanced magnetic fluctuations in the plasma near these thresholds, suggesting that the instabilities are driving the growth of waves. In the case of spring, no definitive assessment is possible due to the corresponding thresholds being so similar at higher $\beta_{||p}$.

The examination of the PDF of magnetic field increments in Figure 4, reveals the appearance of extended tailed PDFs on kinetic scales. The steepening of the spectra suggests dissipation in this range of scales and is consistent with the directly observed heating in the protons. The non-Gaussianity of the PDF of increments for each season shows that there is a presence of intense, phase correlated fluctuations due to the transfer of energy between contiguous eddies. The intermittency observed shows that a nonlinear, non-homogeneous energy transfer is going on.

Examining Figure 5, the spectral indices for the inertial range during summer time periods were found, on average, to be almost exactly the classic Kolmogorov spectral index. This is apparent in the summer PSD plotted in Figure 5 b). Average spectral indices found for solar wind intervals during the Southern hemisphere fall season were also on average closely aligned with the -5/3 slope. This suggests that we did indeed observe mainly solar wind magnetic turbulence. The plasma encountered during this study also exhibits a power spectrum of magnetic field fluctuations characterized by a power law decay. There is evidence of an inertial range with a slope close to -5/3 present in all seasons. Another feature present in approximately 16% of all intervals are peaks and/or bumps around the H^+ gyrofrequency. The majority seen were during the spring (23%) and summer (22%) seasons (e.g., Figure 5 a). Andrés et al. (2020) found that events near the Martian perihelion showed a clear peak in their PSD near the proton cyclotron frequency f_{ci}. The same can be said for this study.

The results of this preliminary study motivate further investigations into how temperature anisotropy constraints arise in Martian exosphere and how they impact the large-scale evolution of the plasma. More numerous and lengthy time periods are needed to decouple the impact of the Martian exosphere on R_p values. Endeavors to determine systematic differences in temperature anisotropy that can be accounted for by seasonal variability would also be of interest. As MAVEN and other Mars-orbiting spacecraft continue to return valuable observations, queries regarding the properties of turbulence and plasma instabilities upstream of Mars can be resolved.

Acknowledgments

The MAVEN mission has been made possible through NASA sponsorship and the dedicated efforts of NASA Goddard Space Flight Center, LASP, Lockheed Martin, and the MAVEN Technical and Science Teams. The MAVEN data shown are publicly available at the NASA Planetary Data System website (http://ppi.pds.nasa.gov).

References

Andrés, N., Romanelli, N., Hadid, L. Z., Sahraoui, F., DiBraccio, G., & Halekas, J. (2020). Solar wind turbulence around mars: Relation between the energy cascade rate and the proton cyclotron waves activity. *The Astrophysical Journal*, *902*, 134 - 143. doi: https://doi.org/10.3847/1538-4357/abb5a7

Bhattacharyya, D., Clarke, J. T., Chaufray, J. Y., Mayyasi, M., Bertaux, J. L., Chaffin, M. S., … Villanueva, G. L. (2017). Seasonal changes in hydrogen escape from mars through analysis of hst observations of the martian exosphere near perihelion. *Journal of Geophysical Research: Space Physics*, *122*(11), 11,756-11,764. doi: https://doi.org/10.1002/2017JA024572

Bruno, R., & Carbone, V. (2016). *Turbulence in the solar wind.* Springer. doi: 10.1007/978-3-319-43440-7

Connerney, J. E. P., Espley, J., Lawton, P., Murphy, S., Odom, J., Oliversen, R., & Sheppard, D. (2015). The maven magnetic field investigation. *Space Science Reviews*, *195*, 257–291. doi: 10.1007/s11214-015-0169-4

Espley, J. R. (2018). The martian magnetosphere: Areas of unsettled terminology. *Journal of Geophysical Research: Space Physics*, *123*(6), 4521–4525. doi: 10.1029/2018JA025278

Greco, A., Chuychai, P., Matthaeus, W. H., Servidio, S., & Dmitruk, P. (2008). Intermittent mhd structures and classical discontinuities. *Geophysical Research Letters*, *35*(19). doi: https://doi.org/10.1029/2008GL035454

Greco, A., Matthaeus, W. H., Servidio, S., Chuychai, P., & Dmitruk, P. (2009). Statistical analysis of discontinuities in solar wind ace data and comparison with intermittent mhd turbulence. *The Astrophysical Journal*, *691*(2), L111–L114. doi: 10.1088/0004-637x/691/2/l111

Halekas, J. S. (2017). Seasonal variability of the hydrogen exosphere of mars. *Journal of Geophysical Research: Planets*, *122*, 901–911. doi: doi:10.1002/2017JE005306

Halekas, J. S., Ruhunusiri, S., Harada, Y., Collinson, G., Mitchell, D. L., Mazelle, C., … Jakosky, B. M. (2017). Structure, dynamics, and seasonal variability of the mars-solar wind interaction: Maven solar wind ion analyzer in-flight performance and science results. *Journal of Geophysical Research: Space Physics*, *122*(1), 547-578. doi: https://doi.org/10.1002/2016JA023167

Halekas, J. S., Taylor, E. R., Dalton, G., Johnson, G., Curtis, D. W., McFadden, J. P., … Jakosky, B. M. (2015). The solar wind ion analyzer for maven. *Space Science Reviews*, *195*, 125-151. doi: 10.1007/s11214-013-0029-z

Hellinger, P., Trávníček, P., Kasper, J. C., & Lazarus, A. J. (2006). Solar wind proton temperature anisotropy: Linear theory and wind/swe observations. *Geophysical Research Letters*, *33*(9). doi: https://doi.org/10.1029/2006GL025925

Horbury, T. S., Forman, M., & Oughton, S. (2008, Oct). Anisotropic scaling of magnetohydrodynamic turbulence. *Phys. Rev. Lett.*, *101*, 175005. doi: 10.1103/PhysRevLett.101.175005

Howes, G. G. (2008). Inertial range turbulence in kinetic plasmas. *Physics of Plasmas*, *15*(5), 055904. doi: 10.1063/1.2889005

Klein, K. G., & Howes, G. G. (2015). Predicted impacts of proton temperature anisotropy on solar wind turbulence. *Physics of Plasmas*, *22*(3), 032903. doi: 10.1063/1.4914933

Kolmogorov, A. (1941, January). The Local Structure of Turbulence in Incompressible Viscous Fluid for Very Large Reynolds' Numbers. *Akademiia Nauk SSSR Doklady*, *30*, 301-305.

Kolmogorov, A. N. (1941, April). Dissipation of Energy in Locally Isotropic Turbulence. *Akademiia Nauk SSSR Doklady*, *32*, 16.

Luhmann, J. (1992). Comparative studies of the solar wind interaction with weakly magnetized planets. *Advances in Space Research*, *12*(9), 191 - 203. doi: https://doi.org/10.1016/0273-1177(92)90331-Q

Marsch, E., & Tu, C.-Y. (1997). Intermittency, non-gaussian statistics and fractal scaling of mhd fluctuations in the solar wind. *Nonlinear Processes in Geophysics*, *4*(2), 101–124. doi: 10.5194/npg-4-101-1997

Maruca, B. A., Chasapis, A., Gary, S. P., Bandyopadhyay, R., Chhiber, R., Parashar, T. N., ... Strangeway, R. J. (2018). Mms observations of beta-dependent constraints on ion temperature anisotropy in earth's magnetosheath. *The Astrophysical Journal*, *866*, 25-30. doi: https://doi.org/10.3847/1538-4357/aaddfb

Maruca, B. A., Kasper, J. C., & Bale, S. D. (2011). What are the relative roles of heating and cooling in generating solar wind temperature anisotropies? *Physical Review Letters*, *107*, 201101. doi: 10.1103/PhysRevLett.107.201101

Maruca, B. A., Kasper, J. C., & Gary, S. P. (2012). Instability-driven limits on helium temperature anisotropy in the solar wind: Observations and linear vlasov analysis. *The Astrophysical Journal*, *748*, 137-143. doi: 10.1088/0004-637X/748/2/137

Matteini, L., Landi, S., Hellinger, P., Pantellini, F., Maksimovic, M., Velli, M., ... Marsch, E. (2007). Evolution of the solar wind proton temperature anisotropy from 0.3 to 2.5 au. *Geophysical Research Letters*, *34*(20). doi: https://doi.org/10.1029/2007GL030920

Matthaeus, W. H., & Goldstein, M. L. (1982). Measurement of the rugged invariants of magnetohydrodynamic turbulence in the solar wind. *Journal of Geophysical Research*, *87*(A8), 6011-6028. doi: https://doi.org/10.1029/JA087iA08p06011

Mazelle, D. S. K., C.and Winterhalter, Trotignon, J., Acuña, M., Baumgärtel, K., Bertucci, C., Brain, D., ... Slavin, J. (2004). Bow shock and upstream phenomena at mars. *Space Science Reviews*, *111*, 115-181. doi: https://doi.org/10.1023/B:SPAC.0000032717.98679.d0

Munteanu, C., Negrea, C., Echim, M., & Mursula, K. (2016). Effect of data gaps: comparison of different spectral analysis methods. *Annales Geophysicae*, *34*(4), 437–449. doi: 10.5194/angeo-34-437-2016

Osman, K. T., Matthaeus, W. H., Gosling, J. T., Greco, A., Servidio, S., Hnat, B., ... Phan, T. D. (2014). Magnetic reconnection and intermittent turbulence in the solar wind. *Physical Review Letters*, *112*, 215002-215007. doi: 10.1103/PhysRevLett.112.215002

Osman, K. T., Matthaeus, W. H., Hnat, B., & Chapman, S. C. (2012). Kinetic signatures and intermittent turbulence in the solar wind plasma. *Physical Review Letters*, *108*, 261103-261107. doi: 10.1103/PhysRevLett.108.261103

Parashar, T. N., Salem, C., Wicks, R. T., Karimabadi, H., Gary, S. P., & Matthaeus, W. H. (2015). Turbulent dissipation challenge: a community-driven effort. *Journal of Plasma Physics*, *81*(5), 905810513. doi: 10.1017/S0022377815000860

Pine, Z. B., Smith, C. W., Hollick, S. J., Argall, M. R., Vasquez, B. J., Isenberg, P. A., ... McLaurin, M. L. (2020). Solar wind turbulence from 1 to 45 au. iv. turbulent transport and heating of the solar wind using voyager observations. *The Astrophysical Journal*, *900*(2), 91-102. doi: https://doi.org/10.3847/1538-4357/abab12

Ruhunusiri, S., Halekas, J. S., Espley, J. R., Mazelle, C., Brain, D., Harada, Y., ... Howes, G. G. (2017). Characterization of turbulence in the mars plasma environment with maven observations. *Journal of Geophysical Research: Space*

Physics, *122*(1), 656-674. doi: https://doi.org/10.1002/2016JA023456

Salem, C., Mangeney, A., Bale, S. D., & Veltri, P. (2009). Solar wind magnetohydrodynamics turbulence: anomalous scaling and role of intermittency. *The Astrophysical Journal*, *702*(1), 537–553. doi: 10.1088/0004-637x/702/1/537

Slavin, J. A., & Holzer, R. E. (1981). Solar wind flow about the terrestrial planets 1. modeling bow shock position and shape. *Journal of Geophysical Research*, *86*(A13), 11401-11418. doi: https://doi.org/10.1029/JA086iA13p11401

Sorriso-Valvo, L., Carbone, V., Veltri, P., Consolini, G., & Bruno, R. (1999). Intermittency in the solar wind turbulence through probability distribution functions of fluctuations. *Geophysical Research Letters*, *26*(13), 1801-1804. doi: https://doi.org/10.1029/1999GL900270

Verscharen, D., Klein, K. G., & Maruca, B. A. (2019). The multi-scale nature of the solar wind. *Living Reviews in Solar Physics*, *16*(5). doi: https://doi.org/10.1007/s41116-019-0021-0

Wan, M., Oughton, S., Servidio, S., & Matthaeus, W. H. (2010). On the accuracy of simulations of turbulence. *Physics of Plasmas*, *17*(8), 082308. doi: 10.1063/1.3474957

Zimbardo, G., Greco, A., Sorriso-Valvo, L., Perri, S., Vörös, Z., Aburjania, G., … Alexandrova, O. (2010). Magnetic turbulence in the geospace environment. *Space Science Reviews*, *156*, 89-134. doi: 10.1007/s11214-010-9692-5